CHEMISTRY
A EUROPEAN JOURNAL

DOI: 10.1002/chem.200600661

Dissecting the General Physicochemical Properties of Noncovalent Interactions Involving Tyrosine Side Chain as a Second-Shell Ligand in Biomolecular Metal-Binding Site Mimetics: An Experimental Study Combining Fluorescence, ^{13}C NMR Spectroscopy and ESI Mass Spectrometry

Chi Ming Yang,* Xueying Li, Wei Wei, Yitong Li, Zhengjuan Duan, Jianyu Zheng, and Tai Huang[a]

Abstract: Detailed physicochemical features inherent in the dynamic cation–π interactions of aromatic amino acid side chains in the secondary coordination spheres around metal ions were extracted and mapped by intrinsic tyrosine fluorescence titration experiments with two homologous, artificially engineered metal-binding scaffolds which mimic metal-binding sites in metalloproteins. A newly formulated method for the treatment of fluorescence titration data allows straightforward assessment of both the magnitudes and properties of metal-chelation-assisted cation–aromatic interactions (K_2) underlying a proposed two-step metallosupramolecular association process. The unprecedented linear platform-motif correlations between the two contrasting scaffolds in their changes in tyrosine fluorescence on binding of 3d metal cations help to elucidate the properties of general cation–arene recognition corresponding to the metal-responsive characteristics of the second-shell Tyr residue surrounding the metal-binding sites in the supramolecular context, and thereby define a new noncovalent design principle for metal-ion recognition in aqueous solution. As supported by NMR spectroscopic and ESI-MS analyses and molecular mechanics force field calculations, the systematic study exemplifies the concept of using steady-state tyrosine fluorescence as a powerful tool for comprehensive descriptions of cation–π interactions in the extended environment of a metal-binding site. We established that the physicochemical properties pertaining to indirect metal–arene interactions are highly dependent on the electronic properties of the metal ions. This work suggests that second-shell cation-π interactions may play more diverse roles, including modulation of structure, reactivity, and function of metal-binding sites, than the previously well-established direct cation–π interactions involving hard cations (e.g., alkali metal ions). Moreover, such a study will continue to complement theoretical predications and/or the early experimental investigations in organic solvents.

Keywords: cations · fluorescence · ligand design · metalloprotein mimics · pi interactions

Introduction

One of the main challenges facing metalloprotein design is the development of new metal-binding motifs with high selectivity and affinity for metal ions.[1] Rational design of metal-binding motifs for the incorporation of new reactivity and functionality into biomolecules is currently an area of intense interest in the fields of bioorganic and supramolecular chemistry.[1,2]

Artificially constructed biomolecular metal-binding scaffolds composed of unnatural metal-ligating residues to

[a] Prof. Dr. C. M. Yang, X. Li, W. Wei, Y. Li, Z. Duan, Prof. Dr. J. Zheng, T. Huang
Neurochemistry and Physical Organic Chemistry
Nankai University, Tianjin 300071 (China)
Fax: (+86) 22-2350-3863
E-mail: yangchm@nankai.edu.cn
systembiogroup@yahoo.com.cn

Supporting information for this article is available on the WWW under http://www.chemeurj.org/ or from the author.

mirror native-protein metal-binding sites is a powerful approach to achieving new functionality and advancing biological understanding of the structure and function of metalloproteins.[2] Since a delicate amalgamation of various weak interactive forces is pivotal to biomolecular recognition, the design and elucidation of a novel interactive network of molecular recognition units is fundamental to the design of new metal-binding motifs.

Recent investigations in protein design and computational chemistry revealed that weak noncovalent interactions between first-shell (direct) metal ligands and second-shell (indirect) ligands are crucial to the attendant biological functions of metalloproteins.[3,4] Although second-sphere ligand interactions, such as hydrogen bonding, hydrophobic interactions, π stacking, and salt bridges, with first-shell ligating residues of the active sites have been recognized as enhancing binding-site affinity for the metals and modulating the reactivity, both the physicochemical properties and the roles of indirect cation–π noncovalent interactions involving aromatic amino acid side chains in the second coordination sphere of metal ions have remained elusive.

Cation–π interactions are newly identified molecular recognition ingredients which have attracted great research attention within the past few years.[4,5] However, major previous interest has focused on direct cation–π interactions of hard cations with biomolecular aromatics, and the interactions of ammonium and alkali metal ions with aromatic side chains of tyrosine (Tyr, Y) and tryptophan (Trp, W) have been subjected to vigorous research efforts because of their fundamental importance in supramolecular chemistry and biology.[4,5]

In all metalloproteins and metalloenzymes, hydrophobic residues in the second shell include aromatic amino acid side chains surrounding the metal-binding site. Recently, theoretical calculations based on crystallographic data in the protein data bank predicted that cation–π noncovalent interactions of second-shell aromatic amino acid side chains surrounding metal-binding sites are ubiquitous in static metalloprotein structures and can be essential components in diverse metalloproteins.[4,5] Nevertheless, a formidable gap remains between the theoretical aspects[5] of cation–π contacts and the physicochemical basis of such molecular recognition elements in metalloproteins under physiologically relevant conditions, and hence the level at which they are applied in the interpretation of biomolecular structures and functions. In particular, experimental investigations using suitable model systems for biogenic metal-mediated cation–aromatic interactions involving biological-function-associated, second-sphere aromatic side chains in metalloproteins remain largely unexplored.[7] Specifically, experimental attempts to date to define the existence and the nature of the cation–π noncovalent bonding of biomolecular aromatic rings, notably the Tyr side chain, with biologically significant metal ions in aqueous solution has been severely hampered by the multiple competing interactions which often surround cationic centers.[4–8] In fact, the widespread Tyr phenolic side chain moiety is most difficult to study in solution because it can also act as an ambidentate noncovalent ligand for metal ions.

Quantitative determination of ammonium cation–π noncovalent interactions in peptide systems[6k] and host–guest complexes[9a] has been exemplified by various novel experimental approaches by Kostić et al. and Hunter et al., respectively. To investigate cation–arene recognition with a synthetic receptor[9] or sensor,[10] an ideal location of a cation within the motif ensemble is mandatory to ensure specific interaction of an ionic entity with an individual arene moiety of interest. Metalloproteins widely utilize the carboxylate groups of Asp/Glu side chains, the SH groups in Cys, and the amino group(s) in Arg/His residues, along with the ubiquitous carbonyl amide oxygen atom(s) in protein backbones, as direct metal ligands to achieve cooperative intermolecular forces for forming well-organized metal-binding sites within a hydrophilic shell,[3,11] which is frequently surrounded by the functionally multifaceted aromatic amino acid side chains within a larger, hydrophobic shell.[3a,11b]

Multidentate aminocarboxylate ligands such as ethylenediaminetetraacetic acid (EDTA) and diethylenetriaminepentaacetic acid (DTPA) are versatile platforms for the presentation of biomolecular recognition units in the design and investigation of biologically functional molecules.[8] The advantages of employing multidentate aminocarboxylate ligands include the fact that synthetic metal-binding scaffolds and receptors designed on the basis of such platforms are amenable to spectroscopic investigation in aqueous solution. Based on this premise, by using fluorescence techniques in conjunction with multidentate aminocarboxylate platforms in a molecular design, we have recently extended the investigation of weak cation–π interactions of hydrophobic bioaromatic rings to aqueous solution.[8]

As a part of our continuing effort using multidentate aminocarboxylate platforms to elucidate the dynamic metal-responsive properties of aromatic amino acid side chains, herein we describe an unprecedented method for comprehensively extracting the indirect metal–arene recognition properties from artificially designed biometal-binding scaffolds. Our molecular design integrates the versatile yet still controllable coordinating ability of the multidentate aminocarboxylate ligands with the π-electron-donating aptitude of Tyr side-chain aromatic rings, which are preorganized on chelating metal ions by the aminocarboxylate moieties; this provides novel prospects for gaining fundamental insights into the cation–π binding ability of the Tyr phenolic ring as indirect metal ligand.

Methods and Results

Design of metal-binding scaffolds: Two contrasting metal-binding molecules, EDTA-bis(L-Tyr methyl ester), EY_2, and DTPA-bis(L-Tyr methyl ester), DY_2 (Scheme 1) were created as biomolecular metal-binding mimetics for evaluating the intrinsic affinity of the Tyr aromatic ring for divalent metal cations. As outlined in Scheme 1, EY_2 and DY_2 were

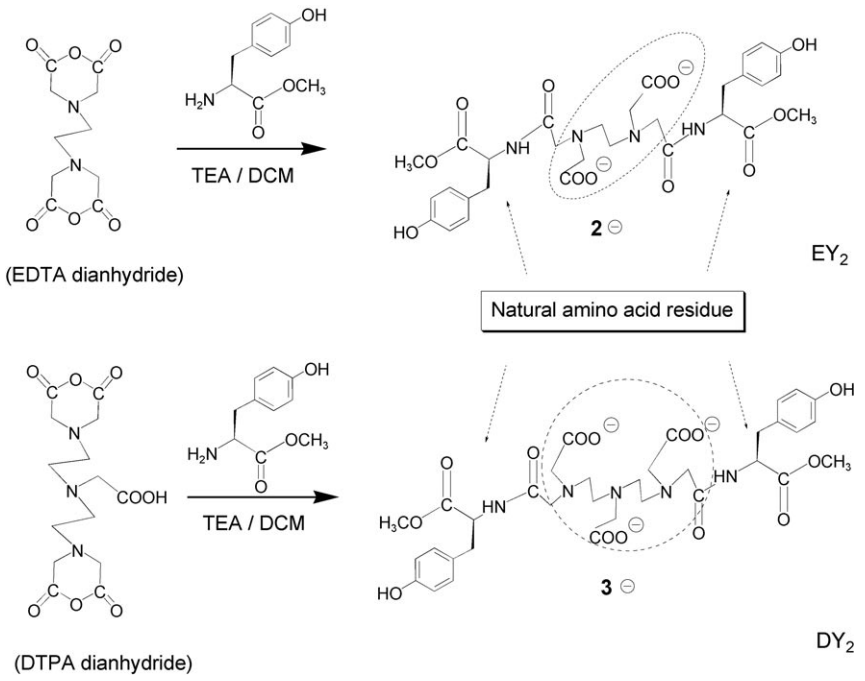

Scheme 1. Synthesis and building blocks of the two metal-binding scaffolds with charge variation in the platforms.

prepared by coupling L-Tyr methyl ester with ethylenediaminetetraacetic dianhydride (EDTA dianhydride) and diethylenetriaminepentaacetic dianhydride (DTPA dianhydride), respectively, according to our previously described procedure,[8] and their identities were established by NMR spectroscopy and MS (see Experimental Section). Molecular scaffold EY_2 comprises two aminocarboxylate chelate moieties for charge complementarity and two Tyr residues tethered to the platform via amide linkages to mimic a binding environment of divalent biometal ions (M^{II}). In scaffold DY_2 a third aminocarboxylate moiety is included for fine-tuning metal coordination while further reducing the tendency of Tyr phenolic hydroxy group to directly bind M^{II}. The use of a combination of complementary binding units in accommodating M^{II} endows the two structurally distinctive molecules with the capability to form various cooperative and competing interactions with the targeted M^{II}, thereby allowing the noncovalent bonding features to be mapped and extracted from the two metal-binding scaffolds, which constitute a charge-balance strategy (Scheme 2).

Spectroscopic methods: Fluorescence and ^{13}C NMR spectroscopy were employed to reliably detect the weak cation–

Scheme 2. Binding of M^{II} ions to the scaffolds. The asterisk designates a noncovalently participating phenolic arene.

π interactions involving the Tyr aromatic ring. Prior to this study, a similar investigative tactic combining fluorescence and ^{13}C NMR spectroscopy proved to be instrumental in successfully extracting the dynamic cation–indole recognition information from the metallosupramolecular association processes of tryptophan-based metal-binding scaffolds.[8]

Fluorescent signaling is one of the most viable approaches to reporting molecular-recognition events.[12–14] With the advent of the fluorescence technique it has become feasible not only to probe precise molecular-recognition information[13] including electrostatic interactions[8,14] of the tryptophan indole ring, but also to dissect enzymatic reaction mechanisms[15] by means of tryptophan fluorescence. Tyrosine fluorescence as a spectroscopic window is also an inviting study candidate, despite its intrinsically low quantum yield.[12d–f,16] The decay of Tyr fluorescence can arise from dynamic processes including electron transfer,[12d] or energy transfer[12e,f] involving the Tyr aromatic ring. Moreover, it is known that Tyr displays a fluorescence lifetime optimal to characterize dynamic motions of biomolecules.[16] The advantages of using the Tyr residue for studies on cation–aromatic interaction include its moderately low fluorescence sensitivity to changes in its surrounding microenvironment. We envisioned that Tyr fluorescence with a moderately low sensitivity, and hence less artifacts, might be beneficial to adequately defining the dynamic physicochemical nature of the noncovalent interactions involving the Tyr aromatic ring with high fidelity. In this regard, steady-state Tyr fluorescence was employed to characterize the metal–ion recognition properties of the scaffolds and to establish the role of the Tyr aromatic ring in the corresponding recognition event.

We demonstrate that sequestering of M^{II} ions from solution by the aminocarboxylate moieties enables the nearby Tyr fluorophore to respond actively and noncovalently to the ligated M^{II} with high selectivity and sensitivity. The cation-responsive property of the Tyr aromatic ring as a second-sphere ligand not only discriminates between various biometal cations having different coordination geometry and number, but also displays a fascinating capacity for variation of the platform. Depending on the electronic properties of M^{II}, distinct metal-controlled cation–π interactive mechanisms, corresponding to characteristic metal-induced fluorescence responses, were revealed.

Fluorescence titration: Among the biologically significant metal ions, Mg^{II}, Ca^{II}, Zn^{II}, Ni^{II}, Co^{II}, Cu^{II}, and Mn^{II} are found most often bound to the active domains in metalloproteins.[11] By monitoring the intrinsic Tyr fluorescence (λ_{ex}/λ_{em} 276/302 nm) in both slightly acidic (pH 4.6) and neutral (pH 7.1)[8,17] buffered water at 25 °C, incremental addition of chloride salts of M^{II} up to one equivalent showed considerable fluorescence emission change of the Tyr chromophore adjacent to the aminocarboxylate chelating sites. The first-row (3d) transition metal[11] ions Cu^{II}, Co^{II}, Ni^{II}, and Mn^{II} lead to fluorescence quenching in a steady-state manner. Intriguingly, the emission change as a result of binding differs distinctly between Zn^{II} (3d metal cation) and Cd^{II} (4d metal cation). For alkaline earth metals as opposed to transition metals, addition of Mg^{II}, like K^{I} and Na^{I}, produces no discernible change in fluorescence emission intensity; however, unlike other M^{II} ions, the presence of Ca^{II} is signaled by a noticeably amplified fluorescence (Figure 1). Remarkably, the metal-responsive property of Tyr in the vicinity of the chelating site in DY_2 is similar to that in EY_2 (Figure 1). Formation of 1:1 complexes between the motif entities and the metals was confirmed by ESI-MS analysis; moreover, negative-ion ESI-MS showed the existence of $[M^{II}(EY_2)Cl]^-$ but not $[M^{II}(DY_2)Cl]^-$ (see Supporting Information), that is, DY_2, as compared to EY_2, was well engineered to further stabilize chelation while retaining comparable fluorescent sensitivity of the Tyr ring to metal binding.

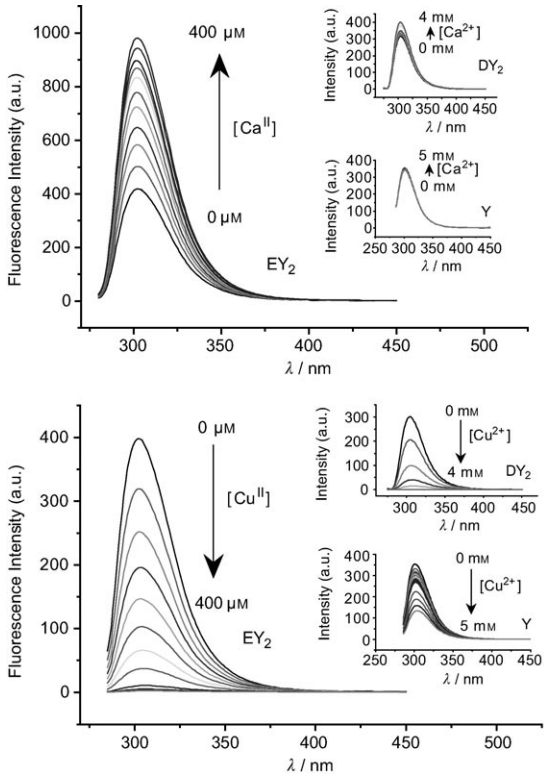

Figure 1. Fluorescence emission changes on incremental addition of Ca^{II} (top) and Cu^{II} (bottom) to a solution of EY_2 (4.0×10^{-4} M) in buffered water at pH 4.6 ± 0.05. Insets: Corresponding changes for DY_2 (4.0×10^{-4} M) and Y (NH_2-Tyr-OMe, 8.0×10^{-4} M).

Static fluorescence quenching, indicative of a strong interaction between a fluorophore and a quencher, is a well-established approach to estimating the affinity of a fluorescent host molecule such as a receptor for a guest entity.[18] Traditionally, the Stern–Volmer equation ($F_0/F=1+K_{SV}[Q]$) or its modified form, the Lehrer plot, is used to analyze the quenching of fluorescence in a single-step supramolecular association process, where F_0 is the fluorescence intensity in the absence of a quencher, F the fluorescence intensity at quencher concentration [Q], and K_{SV} is the Stern–Volmer quenching constant assuming purely dynamic quenching.[18]

To extract and map the weak noncovalent interactions from the metallosupramolecular association processes (Scheme 3), we combined the Stern–Volmer plot and Job

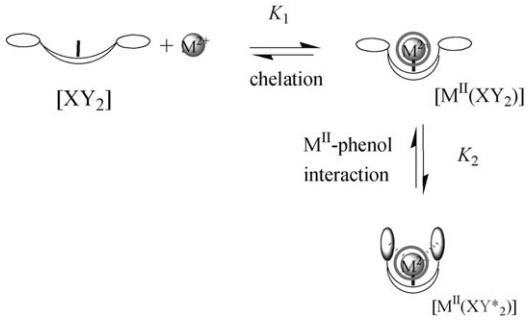

Scheme 3. Sequential two-step supramolecular association.

plot analysis to develop an approximation method for the treatment of fluorescence titration data (see Supporting Information). The newly derived method allowed the straightforward assessment of the magnitudes and properties of metal-chelation-assisted cation–aromatic interactions (K_2) underlying a proposed two-step metallosupramolecular association process, in addition to defining the binding stoichiometry simultaneously.

We use Z to denote the molar fraction of the added metal ions [Eq. (1)], where $[M]_0$ and $[XY_2]_0$ are the initial concentrations of metal ions and metal-binding molecules, respectively.

$$Z=\frac{[M]_0}{[M]_0+[XY_2]_0} \tag{1}$$

For metal ions which are tightly chelated by the aminocarboxylate moieties of the scaffolds, such as transition metal ions, when $0<[M]_0/[XY_2]_0<1$ (i.e., $0<Z<1$) and under equilibrium conditions $[M]_{free}\approx0$, then Equations (2) and (3) can be obtained to describe F/F_0 as a function of Z (see Supporting Information),

$$\left(\frac{F}{F_0}\right)_{EY_2}\cong\left(\frac{1}{1+K_2^{EY_2}}\right)\left(\frac{Z}{1-Z}\right) \tag{2}$$

$$\left(\frac{F}{F_0}\right)_{DY_2} \cong \left(\frac{1}{1+K_2^{DY_2}}\right)\left(\frac{Z}{1-Z}\right) \quad (3)$$

where F is the measured steady-state fluorescence intensity corresponding to the concentration of the overall non-bond-participating Tyr phenolic fluorophore (in both complexed and uncomplexed molecular scaffolds) in the presence of a quencher (metal ions), and F_0 the fluorescence intensity of the scaffolds in the absence of metal ions in solution. The values of K_2 are in accord with the partial association constant arising from the cation–phenol interactions.

When $Z=0.5$ (i.e., at 1:1 molar ratio), Equation (2) is simplified to Equation (4), from which a metal-dependent $K_2^{EY_2}$ was determined from the magnitude of metal-dependent fluorescence change $F/F_0(EY_2)$.

$$\left(\frac{F}{F_0}\right)_{EY_2} \cong \frac{1}{1+K_2^{EY_2}} \quad (4)$$

Similarly, Equation (5) can be obtained, from which a metal-dependent $K_2^{DY_2}$ was determined from the magnitude of metal-dependent fluorescence change $F/F_0(EY_2)$

$$\left(\frac{F}{F_0}\right)_{DY_2} \cong \frac{1}{1+K_2^{DY_2}} \quad (5)$$

Plotting the normalized amplitudes of fluorescence change F/F_0 versus the molar fraction of metal ions, denoted by $Z=[M^{II}]_0/\{[M^{II}]_0+[XY_2]_0\}$, yields the titration curves shown in Figure 2.[8a] We found that the F/F_0 versus Z plot is very useful in straightforwardly evaluating the general cation–aromatic interaction strengths (K_2) underlying the two-step metallosupramolecular association process (see Scheme 3 and Supporting Information).

Three main features derived from the curves in Figure 2 became immediately apparent. First, the fluorescence change approached a maximum at 1:1 molar ratio, that is, each scaffold contains only one binding site for a given divalent metal ion. Second, despite the nearly indistinguishable binding strengths for parent EDTA or related chelate molecules with Cu^{II}, Co^{II}, Ni^{II}, and Zn^{II} ions,[6a,17] the Tyr chromophore in the respective complexes $[M^{II}(XY_2)]$ (X=EDTA, DPTA) exhibits significantly varying changes in fluorescence emission depending on the metal, which closely parallels the previously described behavior of the tryptophan analogue $[M^{II}(XW_2)]$ (X=EDTA, DPTA).[6] Third, based on the assumption of an intimately connected two-step association cascade (Scheme 3), when the molar fraction of added metal ions Z approaches 0.5 (i.e., at 1:1 molar ratio), titration profiles for tightly chelated M^{II} (i.e., when $K_1 \gg K_2$) can in principle be accurately fitted into the theoretical model in Equations (4) and (5) (see Supporting Information), whereby the magnitude of the cation–arene interaction, as given by K_2, are suitably reflected in the fluorescent response.

Platform-motif correlations: The maximum fluorescence change F/F_0 ($\lambda_{ex}/\lambda_{em}$ 276/302 nm) of the metal-binding scaffolds on the addition of 1 equiv of M^{II} at pH 4.6 (100 mM NH_4OAc/HOAc buffer) and pH 7.1 (100 mM Tris-HCl buffer) are summarized in Figure 3.

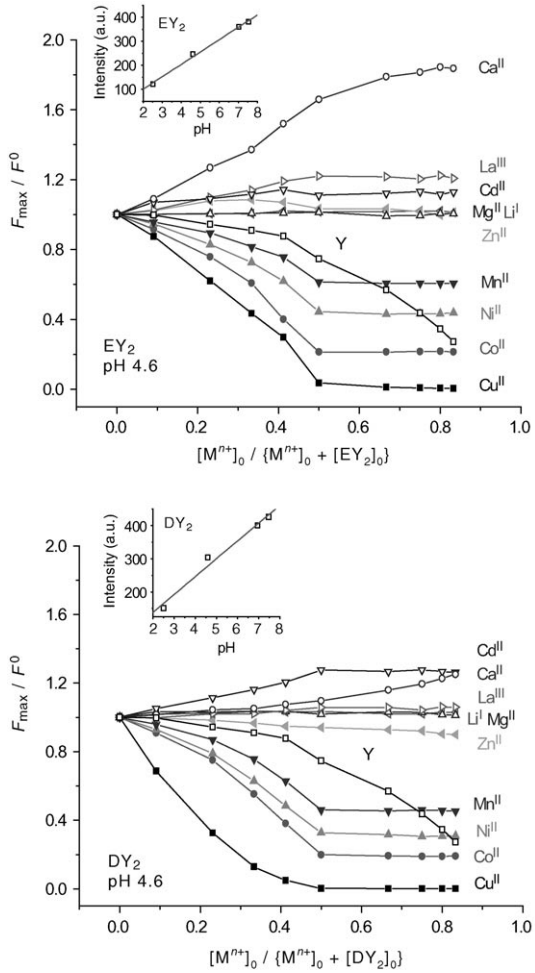

Figure 2. Changes in fluorescence intensities ($\lambda_{ex}/\lambda_{em}$ 276/302 nm) of the metal-binding scaffolds (4.0×10^{-4} M) versus molar fraction of M^{II}. Y: NH_2-Tyr-OMe (8.0×10^{-4} M) titrated with Cu^{II}. Insets: changes in fluorescence intensities of EY_2 and DY_2 with pH.

In depth comparison of the metal-dependent fluorescent change of EY_2 with that of its variant DY_2 can be more transparently described by plotting the maximum fluorescent response $F/F_0(EY_2)$ against $F/F_0(DY_2)$ and, alternatively, F/F_0(pH 4.6) against F/F_0(pH 7.1); see Figure 4. Compelling linear correlations between EY_2 and DY_2 in their optimized responses to the tightly chelated 3d metals (Cu^{II}, Co^{II}, Ni^{II}, Mn^{II}) strongly suggest that a common interaction mechanism, namely, metal-chelation-assisted cation–phenol attraction, is shared by the supramolecular association processes of these metals with EY_2 and its variant DY_2, regardless of one net negative charge in the metallosupramolecular anions $[M^{II}(DY_2)]^-$. The linear plot also revealed that, although M^{II}–aminocarboxylate chelation facilitates the response of the Tyr moiety to the ligated metals, M^{II}–aminocarboxylate chelation is not the feature that directly determines the fluorescence change and thus the magnitude of

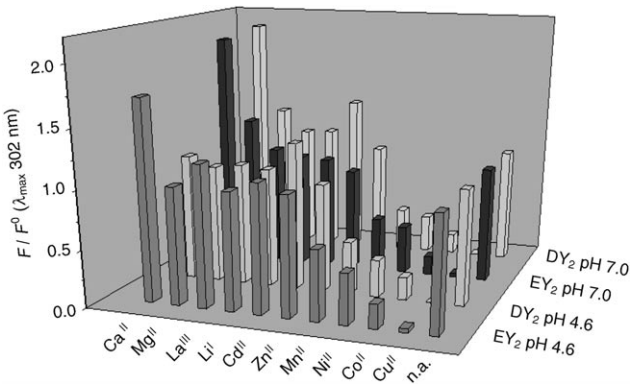

Figure 3. Intrinsic Tyr fluorescence change F/F_0 ($\lambda_{ex}/\lambda_{em}$ 276/302 nm) of the metal-binding scaffolds on the addition of one equivalent of M^{II} at pH 4.6 ± 0.05 (100 mM NH_4OAc/HOAc buffer) and pH 7.1 ± 0.05 (100 mM Tris-HCl buffer).

(pH 4.6). Consequently, within experimental error, both the pH and the platform effects are nearly negligible for these 3d transition metals, as opposed to Cd^{II}, which is a 4d transition metal. The markedly small $\Delta\Delta G°$ values confirm that metal phenolates or ionized phenol are little involved.[20] Specifically, the small $\Delta\Delta G°(EY_2$ vs. $DY_2)$ values reveal that the second shell provides flexibility in the metal environment that permits Tyr side chains in both scaffolds to be equally responsive to the cationic enter.

$$\left(\frac{\left(\frac{F}{F_0}\right)_{DY_2}}{\left(\frac{F}{F_0}\right)_{EY_2}}\right) \cong k \cong \frac{\frac{1}{1+K_2^{DY_2}}}{\frac{1}{1+K_2^{EY_2}}} \cong \left(\frac{1+K_2^{EY_2}}{1+K_2^{DY_2}}\right) \quad (6)$$

The Gibbs free energies corresponding to the chelation-assisted cation–arene recognition are estimated to be 1.97 (Cu^{II}), 0.92 (Co^{II}), 0.48 (Ni^{II}), 0.29 (Mn^{II}), and 0.32 kcal mol^{-1} (Ca^{II}) (EY_2, pH 4.6). For the 3d metal cations (Cu^{II}, Co^{II}, Ni^{II}, Mn^{II}), the magnitudes of interactions based on the fluorescence changes in response to the binding of M^{II} intriguingly parallel the ligand-field stabilization energies of the M^{II} ions, which are Cu^{II} (36.0), Co^{II} (26.6), Ni^{II} (24.3), Mn^{II} (22.3), and Zn^{II} (0).[20,21] The results highlight the importance of the innately different electronic properties of the metals in determining the physicochemical nature of the cation–arene interaction. For paramagnetic metal ions, the magnitudes of the interactions correlate to the oxidative properties of the metal ions, rather than their corresponding affinities to the aminocarboxylate moiety.[19–21] Such a finding has an interesting parallel in the previous demonstration of metal-induced fluorescent responses of the tryptophan analogue EDTA-bis(L-Trp methyl ester), which follow the order $Cu^{II} > Co^{II} > Ni^{II} > Mn^{II}$[8] and were shown to be characteristic of cation–π interactions involving the indole ring. In essence this exceptional resemblance of the results with those obtained with the tryptophan analogues reveal that the centroid of the whole phenol ring as an electron-donor unit, rather than the phenolic oxygen atom of Tyr, predominantly interacts with positively charged entities.

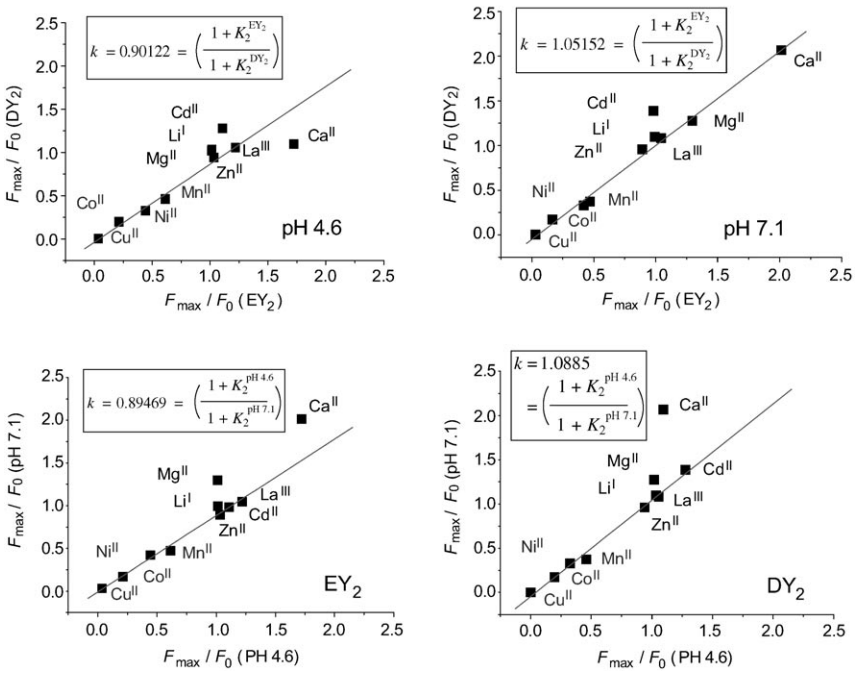

Figure 4. Platform correlations (EY_2 vs. DY_2) at pH 4.6 and 7.1 (top), and pH correlations (pH 4.6 vs 7.1) of EY_2 and DY_2 (bottom) in the metal-induced fluorescence responses F/F_0 ($\lambda_{ex}/\lambda_{em}$ 276/302 nm) of the scaffolds on addition of 1 equiv of M^{II}.

cation–phenol recognition. Rather, the fluorescent responses are attributed to chelation-assisted cation–arene interaction.[8]

Extrapolation from the plots in Figure 4 in accord with the theoretical model in Equation (6) gave the slopes $k =$ 0.895 (EY_2, pH 7.1 vs. 4.6), 1.089 (DY_2, pH 7.1 vs. 4.6), 0.901 (pH 4.6, DY_2 vs. EY_2), and 1.052 (pH 7.1, DY_2 vs. EY_2), which in turn translate into the corresponding Gibbs free energy differences of complex formation (according to $\Delta\Delta G = -RT\ln(K_2^{EY_2}/K_2^{DY_2})$: $\Delta\Delta G°_{EY_2}$(pH 4.6 vs. 7.1) = 0.14, $\Delta\Delta G°_{DY_2}$(pH 4.6 vs. 7.1) = −0.097, $\Delta\Delta G°(EY_2$ vs. $DY_2) = 0.13$ (pH 4.6), and $\Delta\Delta G°(EY_2$ vs. $DY_2) = -0.059$ kcal mol^{-1}

Equally encouraging is the loss of linearity for Ca^{II} and Cd^{II} (Figure 4), indicative of different interactive mechanisms by which the Tyr aromatic ring recognizes alkaline

earth metals and Cd^{II}. We reasoned that, following M^{II}–aminocarboxylate chelation, the increase in fluorescence intensity is conceivably ascribable to intramolecular charge transfer upon electrostatic interactions and polarization[4–6] between the phenolic ring and the Ca^{II}–N^+ bond, which is evidently dependent on the type of platform; while intramolecular electron transfer upon electrostatic interactions and polarization involving the M^{II}–N^+ bond of the paramagnetic M^{II} (Cu^{II}, Co^{II}, Ni^{II}, Mn^{II}), which is nearly independent of the platform, may be a predominant mechanism leading to fluorescence quenching (Figure 4).[20,21]

Since the coordination numbers of the above M^{II} ions are 4–8,[11] the M^{II}–N^+/π interaction (I in Scheme 4) is proposed as the most likely major noncovalent bonding mode.[6] In I the metal-bound tertiary ammonium entity, which has acquired partial positive charge as a result of M^{II}–aminocarboxylate chelation, interacts with the π surface of a second-shell Tyr aromatic side chain. In addition, "charge-assisted" $(HO–H)^{\delta+}/\pi$ (II) and $(CO–NH)^{\delta+}/\pi$ (III) interactions[4,6,7,22] may compete with the M^{II}–N^+/π interactions (I), since, upon metallosupramolecular association, the positive charge on M^{II} is distributed among the metal-bound tertiary N atoms, a putative metal-bound water molecule depending on the buffer and/or pH, and a metal-bound amide moiety (CONH).

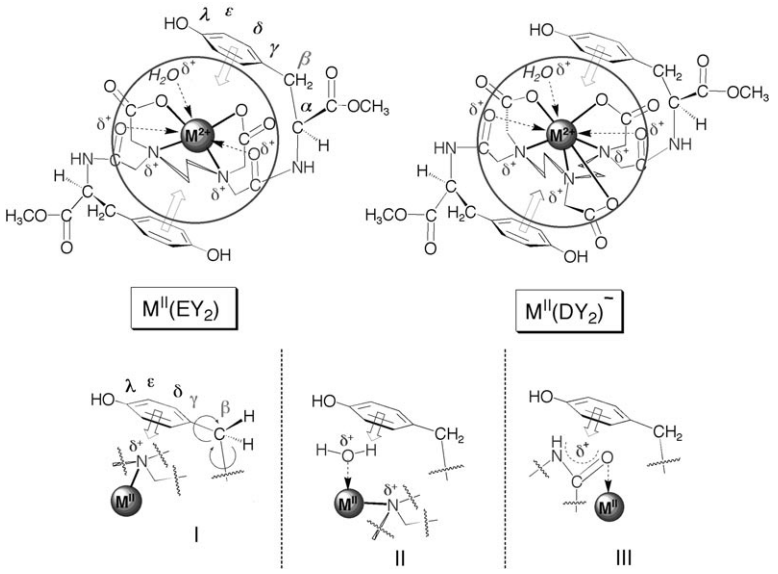

Scheme 4. Putative binding modes: N^+/π interaction (I) is likely favored over $HO^{\delta+}–H/\pi$ (II) and $CO\text{-}N^{\delta+}\text{-}H/\pi$ (III) bonding.

Specifically, the linear platform-motif correlation in Figure 4 is a new, salient phenomenon which strengthens the experimental support for the binding mode in Scheme 4. This finding illustrates that the spectroscopically measured weak interactions most likely arise from direct contact of the metal-bound tertiary ammonium ions with second-shell aryl centroids, and these metal-mediated cation–π interactions are manifested in a dramatically identical manner irrespective of variation in their precise metal-ion-dependent coordination geometries.

In accordance with the bonding model in Scheme 4, force field calculations (MMFF parameters) with Spartan[23] indicate that, in the energy-minimized conformers of $[Ca(EY_2)\cdot H_2O]$ and $[Ca(DY_2)\cdot H_2O]]^-$ complexes, both of the tyrosine side-chain phenol rings are oriented towards the metal center (Figure 5).

Monitoring the dynamic interactions by ^{13}C and ^1H NMR spectroscopy: The above findings are supported by ^{13}C NMR spectroscopic studies, which have proven especially useful in directly and sensitively monitoring dynamic changes in side-chain torsion angles of aromatic amino acids accompanying cation–π interactions.[8b] The ^{13}C (100.7 MHz) and ^1H NMR (400 MHz) spectra resulting from binding of one equivalent of diamagnetic metal ions (Zn^{II}, Cd^{II}, Ca^{II}) to the molecular scaffolds were obtained in D_2O/[D_6]DMSO (1/1). Evidence for metal-binding-mediated cation–π interactions came from the complexation-induced shift in the ^{13}C NMR spectra and line broadening of the ^1H NMR signals of the ligands (Figure 6).

The site-selective shift splitting for the side-chain aromatic signals of the C(δ) and C(ε) positions, in particular, severe signal broadening for the γ-carbon atom of the aryl ring due to the broad distributions of isotropic chemical shifts of equivalent carbon atoms in a biomolecular binding equilibrium, demonstrates that the Tyr phenolic ring experiences dynamic reorientation arising from synchronous cation–π contacts with the M^{II}–N^+ bond. Especially notable is the clear absence of shift change of the C(λ) resonance, indicative of an intact phenolic hydroxyl group.[24] Supporting this view,

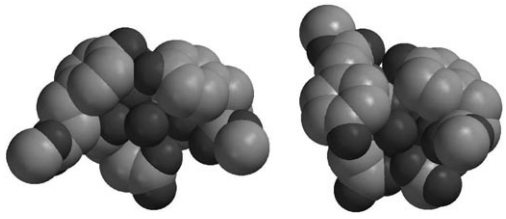

Figure 5. Energy-minimized conformer structures of $[Ca(EY_2)\cdot H_2O]$ and $[Ca(DY_2)\cdot H_2O]]^-$ complexes. The Ca^{II} ion is surrounded by two tyrosine side chains. Hydrogen atoms have been removed for clarity (Spartan 04, Molecular Mechanics MMFF).[21]

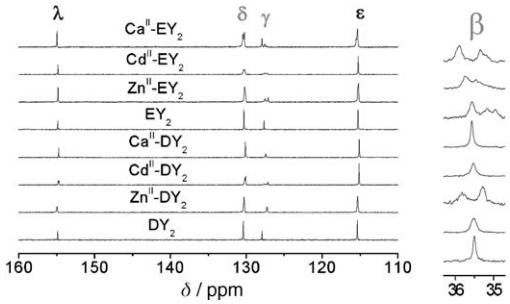

Figure 6. Partial ^{13}C NMR spectra (aromatic region and benzylic CH_2 carbon atoms) of the metal-binding scaffolds (70 mM) on the addition of one equivalent of M^{II} in D_2O/[D_6]DMSO (1/1), pH 4.6.

the rapid orientational change of the aromatic rings as a consequence of the electrostatically favorable noncovalent bonding led to a considerable splitting of the β-CH_2 ^{13}C shift, suggestive of a conformationally twisted aromatic plane. The distinct variations in the ^{13}C NMR splitting patterns caused by association of various M^{II} with the scaffolds are evidence for the aromatic rings being located mainly in immediate proximity to the cations (Scheme 4). The confined orientation of the Tyr side chain associated with the noncovalent interactions is further indicated by significant line broadening of the proton resonance at both the δ and ε positions, with no appreciable net shift change, in the ^{1}H NMR (400 MHz) spectra (see Supporting Information). Moreover, both ^{1}H and ^{13}C NMR spectra of the M^{II}–XY_2 complexes exhibit only one set of signals, in agreement with adoption of an average C_2-symmetric conformation of the supramolecular entity in solution. In a control experiment with NH_2-Tyr-OMe (Y), by contrast, a similar NMR spectroscopic change was not detectable in the presence of Ca^{II} (see Supporting Information), which corroborates results from the fluorescence titration. Additionally, the roles of both the backbone amide carbonyl and the carboxylate oxygen atoms in binding were established by ^{13}C NMR analysis, which revealed predominantly monodentate coordination mode of the carboxylate groups (see Supporting Information).[3d,8b,11d,25] In the ^{13}C NMR spectra selective signal broadening of the methylene groups next to the aminocarboxylate moieties are indicative of direct metal binding to the tertiary amino groups in the scaffolds (see Supporting Information).

Discussion and Conclusion

Both first–second shell weak interactions and cation–aromatic contacts are novel molecular-recognition elements, and both are believed to be closely associated with the structure and function of metalloproteins.[3,4] Since experimental model investigations on the weak interactions surrounding metal-binding sites remain a challenge due to the complexity and diversity of weak interactions in the context of metalloproteins, both the scope and properties of first–second shell cation–π interactions relevant to biomolecules are far from well understood.

By using the peptidyl Tyr chromophore in artificially designed metal-binding scaffolds based on two multidentate aminocarboxylate ligands (EDTA and DTPA), the two contrasting metal-binding molecules were shown to be capable of not only spectroscopically distinguishing among most of the biologically important metal ions in water, but also allow the general physicochemical nature of the cation–π interactions involving second-sphere aromatic rings to be extracted by means of intrinsic Tyr fluorescence titration experiments.

The present study has established a direct relationship between the electronic properties of the metal ions and the cation-recognition properties of the Tyr phenolic side chain in the second coordination sphere, whereby metal–arene interactions in the complexes of Tyr-based scaffolds resemble that seen in metal–indole recognition of the Trp-based scaffolds.[8] Although individual energetic contributions to the secondary ligand interactions may include $(HO{-}H)^{\delta+}/\pi$ (II) and $(CO{-}NH)^{\delta+}/\pi$ (III) bonding in addition to the M^{II}–N^+/π interactions, the unprecedented linear platform-motif correlations between the two homologous scaffolds in their changes in intrinsic Tyr fluorescence on 3d metal binding help dissect the overall physicochemical properties of cation–arene recognition. Importantly, the metal-dependent spectroscopic responses of the scaffolds are found to strictly correlate to the inherent electronic properties of the metal ions, rather than the corresponding aminocarboxylate metal-binding affinities, and this illustrates the use of fluorescence techniques as a powerful tool for physicochemical description of through-space, noncovalent interactions in solution.

^{13}C NMR spectroscopic measurements further established the weak noncovalent interactions of the phenol ring with the cationic entities resulting from diamagnetic metal chelation by the scaffolds in aqueous solution. The altered ^{13}C NMR signals of the aromatic ring reflected the distinct metal-dependent changes in the aromatic ring environments on metal binding to the scaffolds.

As the remarkable preference for involvement of the aryl ring in the cation–π interactions surrounding the coordinatively saturated M^{II} center was found over a broad range of pH values, fluorescence titration has provided a general evaluation of how elaboration to include second-sphere Tyr rings at cation–π sites permits interesting modification of the metal selectivity of the binding sites.

While the biological significance of cation–π interactions of hard cations (e.g., isolated ammonium ions and alkali metal ions) with aromatic amino acid side chains of Tyr and Trp has been stimulating extensive investigations,[4–7] the present work complements the early experimental investigations of cation–π interactions in organic solvents and/or theoretical predications.[4–6] The findings that the phenolic side chain of Tyr is capable of cation–π interactions within metal-binding sites in water are in full agreement with previous studies on cation–π interactions of ammonium ions with the Tyr ring from several groups.[6] We found that, unlike

direct cation–π interactions of hard cations, the magnitude and physicochemical properties of the second-shell cation–π interactions are highly dependent on the valence electronic properties of the metal ions, as shown by both Tyr fluorescence titration and ^{13}C NMR analysis. Therefore, it is expected that second-shell cation–π interactions may play more diverse roles, including modulation of both the structure and function of protein metal-binding sites, than the previously established cation–π interactions pertaining to hard cations.[5,6]

In conclusion, the present work describes a powerful architectural platform for extracting valuable information on metal-chelation-directed cation–arene recognition from metal-binding scaffolds, and thereby defines a new noncovalent design principle for metal-ion recognition in solution, that is, cation–π interactions of the second-shell residues surrounding the metal-binding sites. Steady-state fluorescence and ^{13}C NMR spectroscopic analyses permitted general cation–arene interactions to be quantitatively characterized, and allowed explicit mechanistic assessment of the cation-responsive characteristics of a second-shell Tyr residue in the metallosupramolecular context. To our knowledge, this is the first demonstration that intrinsic Tyr fluorescence is indeed a suitable tool for providing accurate descriptions of cation–π interactions. The concept of using intrinsic Tyr fluorescence and the spectroscopic correlation between the two scaffolds to delineate the profound nature of cation–arene recognition suggests the feasibility of fluorometric measurements in improving our understanding of the cation–π bonding ability of aromatic chromophores in an extended metal-binding site environment.

It has been suggested that the interactions between first- and second-sphere ligands may play a key role in regulating the structure and function of metalloproteins and should be taken into account in the structure-assisted design of metal-binding sites of metalloproteins in order to obtain desired affinity and specific functions.[3] It is anticipated that such new noncovalent design principles may form the groundwork for the development of novel bioactive metal complexes. Inclusion of such unnatural metal-binding sites as key components in the de novo design of proteins may have potential in engineering a range of unprecedented biological activities into semisynthetic metalloproteins[26] and find application in the development of new biosensors.[10]

Experimental Section

General: L-Tyrosine methyl ester was obtained from Novabiochem Corp. and used as received. EDTA dianhydride, DTPA dianhydride, and [D_6]DMSO were purchased from Aldrich and used as received. D_2O was obtained from Acros. All other solvents and reagents, including dichloromethane (DCM), triethylamine (TEA), methanol, and diethyl ether, were of analytical grade and were dried and purified before use. EDTA-bis(L-tyrosine methyl ester) (EY_2) and DTPA-bis(L-tyrosine methyl ester) (DY_2) were synthesized by following our recently described procedure (see Supporting Information),[8] and their identities were established by NMR spectroscopy and MS. The ^1H and ^{13}C NMR spectra were recorded on a Varian Unity-plus 400 spectrometer. The electrospray ionization mass spectrometer was a Finnigen LCQ-Advantage 10 grade ion-trap LC-MS, and the flow rate of the LC pump was 4 μL min^{-1}. Molecular mechanics force field calculations were carried out with PC Spartan 04.[23]

Characterization of EDTA-bis(L-tyrosine methyl ester) (EY_2): ^1H NMR (400 MHz, D_2O): $\delta = 6.94$–6.97 (d, 4H, aromatic), 6.63–6.66 (d, 4H, aromatic), 4.87–4.91 (dd, 2H, chiral CH), 3.55–3.35 (s, 6H, OCH_3), 2.77–3.21 (m, 12H, CH_2CO and CH_2Ar), 2.46–2.48 ppm (m, 4H, NCH_2CH_2N); ^{13}C NMR (100.7 MHz, 1/1 D_2O/[D_6]DMSO): $\delta = 174.8$, 172.5, 171.3, 156.2 (aromatic), 131.6 (aromatic), 129.0 (aromatic), 116.6 (aromatic), 58.2, 57.2, 54.1, 52.4, 52.1, 35.6 ppm (CH_2Ar); ESI$^+$-MS calcd for $C_{30}H_{38}N_4O_{12}$: m/z 646.2; found: 647.2 [EY_2+H$^+$].

Characterization of DTPA-bis(L-tyrosine methyl ester) (DY_2): ^1H NMR (400 MHz, D_2O): $\delta = 7.03$–7.06 (d, 4H, aromatic), 6.73–6.76 (d, 4H, aromatic), 4.55–4.60 (dd, 2H, chiral CH), 3.64 (s, 6H, OCH_3), 2.99–3.53 (m, 14H, CH_2CO and CH_2Ar), 2.78–2.93 ppm (m, 8H, NCH_2CH_2N); ^{13}C NMR (100.7 MHz, 1/1 D_2O/[D_6]DMSO): $\delta = 176.2$, 172.7, 172.2, 168.8, 156.1 (aromatic), 131.4 (aromatic), 129.1 (aromatic), 116.5 (aromatic), 57.9, 57.8, 54.6, 54.0, 52.6, 52.3, 49.7, 35.5 ppm (CH_2Ar); ESI$^+$-MS calcd for $C_{34}H_{45}N_5O_{14}$: m/z 747.3; found: 748.3 [DY_2+H$^+$].

Characterization of 1:1 complexes of metal ions with EY_2 and DY_2 by electrospray-ionization mass spectroscopy (ESI$^+$-MS and ESI$^-$-MS): Typically, appropriate amounts of $CuCl_2$, $CoCl_2$, $NiCl_2$, $ZnCl_2$ (0.01 mL of 0.1 M solutions of metal ion salts containing 1% NaOAc/HOAc buffer), $MnCl_2$, $CdCl_2$, $MgCl_2$, or $CaCl_2$ were added to a solution of EY_2 or DY_2 (1.0 mL, 1.0×10^{-3} M) in redistilled water and shaken to dissolve. All solutions at about 1×10^{-3} M were prepared for mass spectroscopic analysis of the M^{II}-EY_2 or M^{II}-DY_2 complexes. Both ESI (positive) and ESI (negative) MS results showed that all these metal ions primarily form 1:1 complexes with EY_2 or DY_2.

M^{II}-EY_2 complexes (ESI$^+$-MS): Cu^{II}-EY_2: $C_{30}H_{38}N_4O_{12}Cu$ calcd, 709.2; found, 708.3 [EY_2+Cu^{II}−H$^+$]. Co^{II}-EY_2: $C_{30}H_{38}N_4O_{12}Co$ calcd, 705.2; found, 704.2 [EY_2+Co^{II}−H$^+$]. Ni^{II}-EY_2: $C_{30}H_{38}N_4O_{12}Ni$ calcd, 704.2; found, 703.2 [EY_2+Ni^{II}−H$^+$]. Mn^{II}-EY_2: $C_{30}H_{38}N_4O_{12}Mn$ calcd, 701.2; found, 700.2 [EY_2+Mn^{II}−H$^+$]. Zn^{II}-EY_2: $C_{30}H_{38}N_4O_{12}Zn$ calcd, 710.2; found, 709.2 [EY_2+Zn^{II}−H$^+$]. Cd^{II}-EY_2: $C_{30}H_{38}N_4O_{12}Cd$ calcd, 760.2; found, 759.5 [EY_2+Cd^{II}−H$^+$]. Ca^{II}-EY_2: $C_{30}H_{38}N_4O_{12}Ca$ calcd, 686.2; found, 685.2 [EY_2+Ca^{II}−H$^+$]. Mg^{II}-EY_2: $C_{30}H_{38}N_4O_{12}Mg$ calcd, 670.2; found, 669.7 [EY_2+Mg^{II}−H$^+$].

M^{II}-DY_2 complexes (ESI$^+$-MS): Cu^{II}-DY_2: $C_{34}H_{45}N_5O_{14}Cu$ calcd, 810.2; found, 809.2 [DY_2+Cu^{II}−H$^+$]. Zn^{II}-DY_2: $C_{34}H_{45}N_5O_{14}Zn$ calcd, 811.2, found 810.4 [DY_2+Zn^{II}−H$^+$]. Cd^{II}-DY_2: $C_{34}H_{45}N_5O_{14}Cd$ calcd, 861.2; found, 860.5 [DY_2+Cd^{II}−H$^+$]. Ca^{II}-DY_2: $C_{34}H_{45}N_5O_{14}Ca$ calcd, 787.3; found, 786.4 [DY_2+Ca^{II}−H$^+$]. Mg^{II}-DY_2: $C_{34}H_{45}N_5O_{14}Mg$ calcd, 771.3; found, 770.7 [DY_2+Mg^{II}−H$^+$].

Fluorescence titration experiments: Intrinsic fluorescence titration experiments were conducted on a computer-controlled Varian Cary eclipse fluorescence spectrophotometer (Varian Instruments, Palo Alto, CA) attached to a circulating water bath for thermal regulation. A quartz cell with 1-cm path length in both the excitation and emission directions was used in all the experiments, which were conducted at 25 °C. With the excitation wavelength set at 276.0 nm, fluorescence emission spectra (with maximum at 302 nm) were acquired from 450 to 250 nm in 1 nm increments with an average time of 0.1 s. The excitation and emission slit widths were set at 5 nm. The scan rate was 600 nm min^{-1}. The PMT detector voltage was 600 V. A pH of 7.1 was maintained by using 100 mM Tris-HCl buffer, and a pH of 4.6 by using 100 mM ammonium acetate buffer.

From the fluorescence titration data, apparent overall association constants (Table 1) corresponding to the overall supramolecular association processes for EY_2 and DY_2, respectively, can be estimated from the Lehrer plot (see Supporting Information).[18]

For straightforward assessment of the metal-chelation-mediated cation–aromatic interactions (K_2), a new data treatment method was derived (see Supporting Information).

Table 1. Apparent overall association constants K_a [M^{-1}] at 25 °C. The bindings of the rest of the metal ions were too weak to estimate accurate values.

	EY_2, pH 4.6	EY_2, pH 7.1	DY_2, pH 4.6	DY_2, pH 7.1
Cu^{II}	6.48×10^7	5.96×10^8	1.01×10^9	6.76×10^9
Co^{II}	4.26×10^6	3.02×10^7	2.26×10^7	6.56×10^7
Ni^{II}	1.13×10^6	2.31×10^6	4.75×10^6	7.49×10^6
Mn^{II}	2.61×10^5	1.03×10^6	1.04×10^6	1.35×10^6
Ca^{II}	2.33×10^4	9.27×10^4	4.05×10^5	3.19×10^6

Syntheses, fluorescence titration, derivations of methods for data treatment, ESI-MS and NMR spectra are available as Supporting Information.

Acknowledgements

This work was supported by basic research grants from the NSFC (Nos. 20472029; 20421202) and the Ministry of Sci. & Tech. (Nos. 2000-35; 2001-51). The authors thank Professors Xinsheng Wang, Xiaohua Xu, Xianhe Bo, and Dr. Shuzhong Zhang for instrumental support, Professors Zhengming Li, Ruyu Chen, Huazheng Yang, Shansheng Xu, Yongmei Wang, Baiquan Wang, Fangzhong Hu, and Liangfu Tang for friendly assistance, and the reviewers for insightful suggestions.

[1] a) D. E. Benson, M. S. Wisz, H. W. Hellinga, *Curr. Opin. Chem. Biol.* **1998**, *2*, 370; b) L. Regan, *Trends Biochem. Sci.* **1995**, *20*, 280; c) J. T. Kellis, Jr., R. J. Todd, F. H. Arnold, *Nat. Biotechnol.* **1991**, *9*, 994.

[2] a) F. Ruan, Y. Chen, P. B. Hopkins, *J. Am. Chem. Soc.* **1990**, *112* , 9403; b) B. Imperiali, S. L. Fisher, *J. Am. Chem. Soc.* **1991**, *113*, 8527; c) R. P. Cheng, S. L. Fisher, B. Imperiali, *J. Am. Chem. Soc.* **1996**, *118*, 11349.

[3] a) S. Karlin, Z.-Y. Zhu, K. D. Karlin, *Proc. Natl. Acad. Sci. USA* **1997**, *94*, 14225; b) S. F. Marino, L. Regan, *Chem. Biol.* **1999**, *6*, 649; c) G. Xing, V. J. DeRose, *Curr. Opin. Chem. Biol.* **2001**, *5*, 196; d) T. Dudev, Y.-l. Lin, M. Dudev, C. Lim, *J. Am. Chem. Soc.* **2003**, *125*, 3168; e) L. L. Kiefer, S. A. Paterno, C. A. Fierke, *J. Am. Chem. Soc.* **1995**, *117*, 6831; f) J. T. Welch, W. R. Kearney, S. J. Franklin, *Proc. Natl. Acad. Sci. USA* **2003**, *100*, 3725; g) C. A. DiTusa, K. A. McCall, T. Christensen, M. Mahapatro, C. A. Fierke, E. J. Toone, *Biochemistry* **2001**, *40*, 5345; h) F. L. Gervasio, V. Schettino, S. Mangani, M. Krack, P. Carloni, M. Parrinello, *J. Phys. Chem. B* **2003**, *107*, 6886; i) Y. Lu, J. S. Valentine, *Curr. Opin. Struct. Biol.* **1997**, *7*, 495.

[4] a) S. D. Zarić, D. M. Popović, E.-W. Knapp, *Chem. Eur. J.* **2000**, *6*, 3935; b) O. Yamauchi, A. Odani, M. Takani, *J. Chem. Soc. Dalton Trans.* **2002**, *18*, 3411; c) S. D. Zarić, *Eur. J. Inorg. Chem.* **2003**, 2197.

[5] a) J. C. Ma, D. A. Dougherty, *Chem. Rev.* **1997**, *97*, 1303; b) E. A. Meyer, R. K. Castellano, F. Diederich, *Angew. Chem.* **2003**, *115*, 1244; *Angew. Chem. Int. Ed.* **2003**, *42*, 1210; c) G. W. Gokel, L. J. Barbour, R. Ferdani, J. Hu, *Acc. Chem. Res.* **2002**, *35*, 878.

[6] a) K. S. Kim, J. Y. Lee, S. J. Lee, T.-K. Ha, D. H. Kim, *J. Am. Chem. Soc.* **1994**, *116*, 7399; b) S. Mecozzi, A. P. West, Jr., D. A. Dougherty, *J. Am. Chem. Soc.* **1996**, *118*, 2307; c) E. Cubero, F. J. Luque, M. Orozco, *Proc. Natl. Acad. Sci. USA* **1998**, *95*, 5976; d) A. Pullman, G. Berthier, R. Savinelli, *J. Am. Chem. Soc.* **1998**, *120*, 8553; e) S. Roelens, R. Torriti, *J. Am. Chem. Soc.* **1998**, *120*, 12443; f) O. M. Cabarcos, C. J. Weinheimer, J. M. Lisy, *J. Chem. Phys.* **1999**, *110*, 8429; g) J. P. Gallivan, D. A. Dougherty, *Proc. Natl. Acad. Sci. USA* **1999**, *96*, 9459; h) J. B. Nicholas, B. P. Hay, *J. Phys. Chem. A* **1999**, *103*, 9815; i) R. C. Dunbar, *J. Phys. Chem. A* **2000**, *104*, 8067; j) S. L. De Wall, E. S. Meadows, L. J. Barbour, G. W. Gokel, *Proc. Natl. Acad. Sci. USA* **2000**, *97*, 6271; k) E. V. Pletneva, A. T. Laederach, D. B. Fulton, N. M. Kostić, *J. Am. Chem. Soc.* **2001**, *123*, 6232; l) S. Bartoli, S. Roelens, *J. Am. Chem. Soc.* **2002**, *124*, 8307; m) Y. Mo, G. Subramanian, J. Gao, D. M. Ferguson, *J. Am. Chem. Soc.* **2002**, *124*, 4832; n) C. Ruan, M. T. Rodgers, *J. Am. Chem. Soc.* **2004**, *126*, 14600.

[7] a) N. J. van der Veen, R. J. M. Egberink, J. F. J. Engbersen, F. J. C. M. van Veggel, D. N. Reinhoudt, *Chem. Commun.* **1999**, 681; b) H. Kumita, T. Kato, K. Jitsukawa, H. Einaga, H. Masuda, *Inorg. Chem.* **2001**, *40*, 3936; c) O. Yamauchi, A. Odani, S. Hirota, *Bull. Chem. Soc. Jpn.* **2001**, *74*, 1525.

[8] a) Y. Li, C. M. Yang, *Chem. Commun.* **2003**, *23*, 2884; b) Y. Li, C. M. Yang, *J. Am. Chem. Soc.* **2005**, *127*, 3527.

[9] a) C. A. Hunter, C. M. R. Low, C. Rotger, J. G. Vinter, C. Zonta, *Proc. Natl. Acad. Sci. USA* **2002**, *99*, 4873; b) H.-J. Schneider, *Angew. Chem.* **1991**, *103*, 1419; *Angew. Chem. Int. Ed. Engl.* **1991**, *30*, 1417; ; c) S. L. Tobey, E. V. Anslyn, *J. Am. Chem. Soc.* **2003**, *125*, 14807.

[10] a) A. W. Czarnik, *Chem. Biol.* **1995**, *2*, 423; b) S. C. Burdette, S. J. Lippard, *Coord. Chem. Rev.* **2001**, *216*, 333.

[11] a) *Handbook on Metalloproteins* (Eds.: I. Bertini, A. Sigel, H. Sigel), Marcel Dekker, New York, **2001**; b) M. M. Yamashita, L. Wesson, G. Eisenman, D. Eisenberg, *Proc. Natl. Acad. Sci. USA* **1990**, *87*, 5648; c) R. J. P. Williams, *Chem. Commun.* **2003**, 1109; d) T. Dudev, C. Lim, *Chem. Rev.* **2003**, *103*, 773.

[12] a) J. A. Poveda, M. Prieto, J. A. Encinar, J. M. Gonzalez-Ros, C. R. Mateo, *Biochemistry* **2003**, *42*, 7124; b) P. Damberg, J. Jarvet, P. Allard, Ü. Mets, R. Rigler, A. Gräslund, *Biophys. J.* **2002**, *83*, 2812; c) H. Yagi, K. Tozawa, N. Sekino, T. Iwabuchi, M. Yoshida, H. Akutsu, *Biophys. J.* **1999**, *77*, 2175; d) P. Gauduchon, Ph. Wahl, *Biophys. Chem.* **1978**, *8*, 87; e) R. Cowgill in *Biochemical Fluorescence: Concepts, Vol. 2* (Eds.: R. F. Chen, H. Edelhoch), Marcel Dekker, New York, **1976**, pp. 441–487; f) J. B. A. Ross, W. R. Laws, K. W. Rousslang, H. R. Wyssbrod in *Topics in Fluorescence Spectroscopy, Biochemical Applications, Vol. 3* (Ed.: J. R. Lakowicz), Plenum Press, New York, **1992**, pp. 1–63.

[13] a) B. Liu, R. K. Thalji, P. D. Adams, F. R. Fronczek, M. L. McLaughlin, M. D. Barkley, *J. Am. Chem. Soc.* **2002**, *124*, 13329; b) A. H. A. Clayton, W. H. Sawyer, *Biophys. J.* **1999**, *76*, 3235.

[14] J. T. Vivian, P. R. Callis, *Biophys. J.* **2001**, *80*, 2093.

[15] C. Castro, A. A. Gratson, J. C. Evans, J. Jiracek, M. Collinsova, M. L. Ludwig, T. A. Garrow, *Biochemistry* **2004**, *43*, 5341.

[16] S. T. Ferreira, L. Stella, E. Gratton, *Biophys. J.* **1994**, *66*, 1185.

[17] To avoid metal phenoxylate formation and hydrolysis of metal salts and to eliminate effects of ionic strength variation, a slightly acidic buffer (pH 4.6) with a high electrolyte concentration was chosen. Effect of elevated pH (7.1) was examined to display its relevance to biological systems.

[18] a) A. K. Sau, C.-A. Chen, J. A. Cowan, S. Mazumdar, S. Mitra, *Biophys. J.* **2001**, *81*, 2320; b) R. M. Jones, L. Lu, R. Helgeson, T. S. Bergstedt, D. W. McBranch, D. G. Whitten, *Proc. Natl. Acad. Sci. USA* **2001**, *98*, 14769; c) S. Pal, S. Chandra, S. Chowdhury, D. Sarkar, A. N. Ghosh, C. D. Gupta, *J. Biol. Chem.* **1999**, *274*, 32771; d) S. Bourot, O. Sire, A. Trautwetter, T. Touzé, L. F. Wu, C. Blanco, T. Bernard, *J. Biol. Chem.* **2000**, *275*, 1050; e) K. K. Khan, S. Mazumdar, S. Modi, M. J. Sutcliffe, G. C. K. Roberts, S. Mitra. *Euro. J. Biochem.* **1997**, *244*, 361; f) R. Lange, P. Anzenbacher, S. Muller, L. Maurin, C. Balny, *Eur. J. Biochem.* **1994**, *226*, 963; g) J. Sung, K. J. Shin, S. Lee, *Chem. Phys.* **1994**, *179*, 23; h) S. S. Lehrer, *Biochemistry* **1971**, *10*, 3254.

[19] Stability constants (pK_s, 25 °C) of EDTA complexation with metal ions are: Cu^{II} (18.8), Co^{II} (16.3), Ni^{II} (18.6), Mn^{II} (13.9), Zn^{II} (16.5), Ca^{II} (10.7), and Mg^{II} (8.7).

[20] pK_a (Tyr OH) = 9.11–10.1; E_{ox}(PhOH/PhO$^{\bullet}$) = 0.86 V (at pH 7 in water) versus NHE (A. Harriman, *J. Phys. Chem.* **1987**, *91*, 6102). Direct bonding of the OH bond dipole of the phenolic hydroxy group with metal ions is not coordinatively required, and bonding of the phenolic hydroxy group with either metal-bound water or metal-bound tertiary ammonium ion is very unlikely in the metal scaffold XY_2.[6]

[21] a) The interactive strength is highly dependent on the second ionization potential (IP) of the first-row transition metals. Copper has the highest second IP of any of the 3d transition metals: M. T. Rodgers, P. B. Armentrout, *Acc. Chem. Res.* **2004**, *37*, 989. b) We have Zn^{II} (d^{10}), Mn^{II} (d^5), Co^{II} (d^7), Ni^{II} (d^8), and Cu^{II} (d^9) in high-spin states. The fluorescence changes in response to the binding of M^{II} parallel the relative ligand-field stabilization energies of the M^{II} ions: Cu^{II} (36.0), Co^{II} (26.6), Ni^{II} (24.3), Mn^{II} (22.3), and Zn^{II} (0) (the relative ratios of values in water) (D. Asthagiri, L. R. Pratt, M. E. Paulaitis, S. B. Rempe, *J. Am. Chem. Soc.* **2004**, *126*, 1285.)

[22] a) A. Wlodawer, J. Walter, R. Huber, L. Sjölin, *J. Mol. Biol.* **1984**, *180*, 301; b) M. Perutz, *Philos. Trans. R. Soc. London Ser. A* **1993**, *345*, 105; c) G. Tóth, R. F. Murphy, S. Lovas, *J. Am. Chem. Soc.* **2001**, *123*, 11782.

[23] Spartan 04 for Windows, Wave function Inc., Irvine, CA.

[24] a) ^{13}C NMR assignment was made on the basis of APT experiments (see Supporting Information) and literature data. b) Ionization of the phenolic hydroxy groups was not observed. Ionization of the phenolic hydroxy groups of tyrosine residues in peptides and proteins would produce appreciable shifts of the C(λ) ^{13}C nuclear magnetic resonance: R. S. Norton, J. H. Bradbury, *J. Chem. Soc. Chem. Commun.* **1974**, 870b.

[25] a) ^{13}C NMR spectroscopic determination of bidentate vs monodentate coordination of a carboxylate group: B.-H. Ye, X.-Y. Li, I. D. Williams, X.-M. Chen, *Inorg. Chem.* **2002**, *41*, 6426; b) T. Dudev, C. Lim, *J. Phys. Chem. A* **2004**, *108*, 4546.

[26] a) Y. Lu, S. M. Berry, T. D. Pfister, *Chem. Rev.*, **2001**, 101, 3047; b) C. M. Thomas, T. R. Ward, *Chem. Soc. Rev.* **2005**, *34*, 337.

Received: May 11, 2006
Revised: October 27, 2006
Published online: January 3, 2007

